Nanoscale

Accepted Manuscript

This article can be cited before page numbers have been issued, to do this please use: Y. Qiu, Y. Zhao, X. Yang, W. Li, Z. Wei, Q. Lin, J. Xiao, S. Leung, H. Wu, Y. Zhang, Z. Fan and S. Yang, *Nanoscale*, 2014, DOI: 10.1039/C3NR06675D.

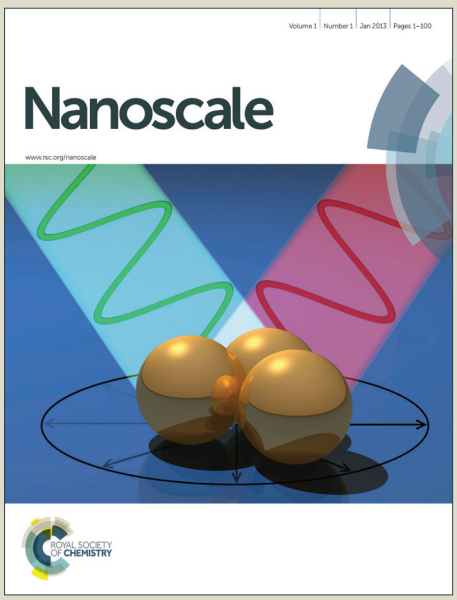

ROYAL SOCIETY OF CHEMISTRY

www.rsc.org/nanoscale

Dynamic Article Links ▶
View Article Online
DOI: 10.1039/C3NR06675D

Cite this: DOI: 10.1039/c0xx00000x

www.rsc.org/xxxxxx

ARTICLE TYPE

Three-dimensional metal/oxide nanocone arrays for high-performance electrochemical pseudocapacitors

Yongcai Qiu,[†,‡,§] Yihua Zhao,[†] Xiaowei Yang,[§] Wanfei Li,[§] Zhanhua Wei,[†] Junwu Xiao,[†] Siu-Fung Leung,[‡] Qingfeng Lin,[‡] Hongkai Wu,[†] Yuegang Zhang,[§,*] Zhiyong Fan,[‡,*] Shihe Yang[†,*]

Received (in XXX, XXX) Xth XXXXXXXXX 20XX, Accepted Xth XXXXXXXXX 20XX
DOI: 10.1039/b000000x

Three-dimensional (3D) electrodes are critical to enabling high-performance power sources. We report here on the design and fabrication, by combining imprint and soft-printing technologies, of 3D nanocone arrays as a novel platform for high performance pseudocapacitors. Such purpose-built 3D nanocone arrays have the advantages of simplicity/versatility/reliability of fabrication, generality to a vast range of active materials, high electrode surface area, and easy electrolyte permeation. As a demonstration of principle, Au and MnO_2 were sequentially deposited forming a 3D Au/MnO_x nanocone array electrode for a pseudocapacitor device. This device obtained a specific mass (areal) capacitance of 840.3 F g^{-1} (88.2 mF cm^{-2}) at a current density of 2 A g^{-1}. Additionally, the asymmetric supercapacitor using the Au/MnO_x nanocone array as the positive electrode and a carbon–based material as the negative electrode achieved a capacitance of 108.5 F g^{-1} at a current density of 1 A g^{-1}, corresponding to an energy density of as high as 46.8 Wh Kg^{-1} at a power density of 0.72 kW Kg^{-1}. The cell still preserved 96.5% of the initial capacitance even after 2000 cycles at a current density of 2 A g^{-1}. The initial result is at least on a par with those of the best asymmetric supercapacitors reported so far, and thus bolsters the development value of the conductive nanocone arrays for high-performance supercapacitors and other energy-storage devices.

Electrochemical energy storage devices, i.e., supercapacitors and Li-ion batteries, have attracted great attention over the past few years.[1-4-4] Comparatively, supercapacitors are superior to Li-ion batteries in terms of fast charge/discharge rates, high power densities, long lifetimes and a good safety record.[4,5] However, the rather low energy densities of supercapacitors have so far largely limited their practical applications due mainly to their small surface area dependent capacitance and narrow operating potential window.[4-5] To resolve these problems, various architectures such as nanowires, nanotubes and carbon textiles have been utilized as binder-free electrodes.[2,6,20,21] for the directly deposition of pseudocapacitive materials. However, the capacitance achieved thus far is still lower than the corresponding theoretical expectation. A more promising strategy perhaps rests

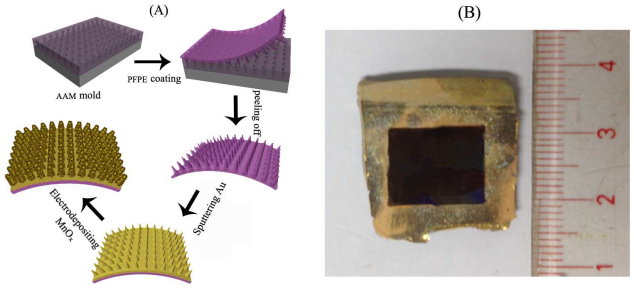

Figure 1. **Fabrication of the 3D metal/oxide nanocone array electrode.** A, Schematic diagram of the fabrication process of the 3D flexible nanocone array electrode. B, Optical image of an as-prepared 3D MnO_x/Au nanocone array electrode.

in the *de novo* design and fabrication of ordered 3D conductive architectures, which has been, if any, much less explored. Such a 3D nanostructured electrode should not only largely shorten electron transportation distance but also allow easy access of the electrolytes to the electrochemically active materials, making it especially important for pseudocapacitors.

Metal oxides or hydroxides such as MnO_2, NiO, CoO_x, FeO_x, RuO_2 and $Ni(OH)_2$, have been widely used as electrode materials owing to their high pseudocapacitance,[6-16] much higher than those of the carbon-based materials in electric double-layer capacitors. Among these active electrode materials, MnO_x has the advantages of low cost, environmental benignity and high theoretical capacitance of >1300 F g^{-1}. [17-18] Despite the use of some nanostructureed electrodes for capacitance enhancement,[2,19-21] the performance of MnO_x-based supercapacitors at high charge/discharge rates is still far from satisfactory due mainly to low electric conductivity of the active material. To tackle this problem, we have engineered a simple ordered architecture, namely a 3D metal/oxide nanocone array, for the supercapacitor electrodes. The 3D nanocone array builds on two pivotal developments: the imprint-assisted electrochemical fabrication of the inverted nanocone hole array architecture as a template for contact-printing and the controllable electrodeposition of pseudo-capacitive materials atop. Measurements have revealed excellent electrochemical performance of the purpose-built 3D metal/oxide nanocone array electrodes, including high capacitance, high energy density and long cycle lifetime.

Our first attempt was to produce a square lattice of nanocone array based on our recent success to fabricate such template

View Article Online
DOI: 10.1039/C3NR06675D

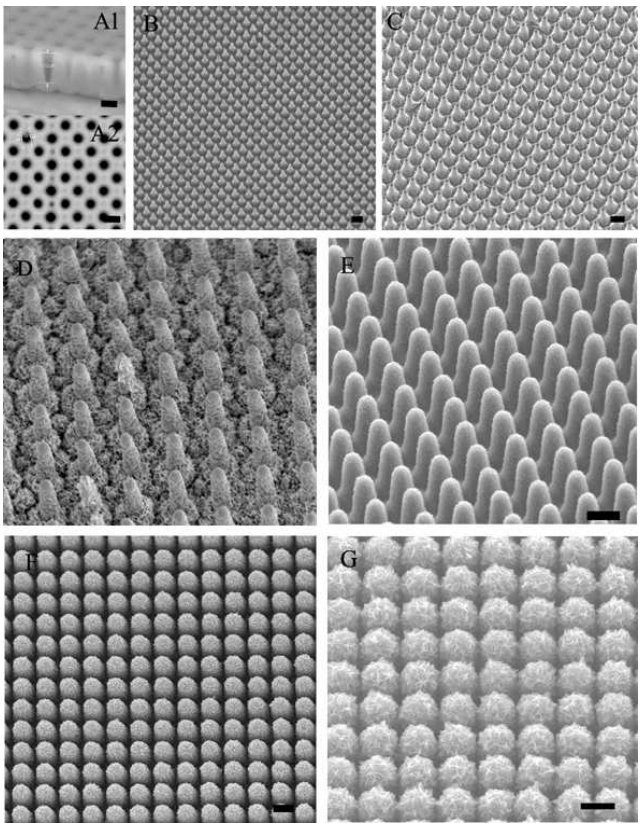

***Figure 2*. Microscopy characterizations of the 3D nanocone arrays at different stages of the pattern transfer and outer layer deposition.** A, Cross-sectional (A_1) and top (A_2) SEM images of an as-prepared nanocone array mold with a height of ~1.7 μm and an open-diameter of ~580 nm. B, SEM image of a desired PTPE nanocone array obtained from the mold A. C, A metal nanocone array electrode obtained by magnetron sputtering Au. D, E, F and G, Electrodeposition of MnO_x on Au metal nanocone array electrode in different time of 70 s, 175 s, 350 s and 700 s, respectively. All scare bars: 1 μm.

assisted by imprint, which can lead to geometrically precisely controlled 3-D structures.[22-23] The fabrication of the 3D Au/MnO_x nanocone array electrode involved mainly four steps: i) nanoimprint-assisted electrochemical preparation of a template with an inverted nanocone hole array; ii) transfer of the inverted nanocone hole array into a normal nanocone array by polymer contact printing; iii) sputtering deposition of a thin layer of highly conductive Au metal on the polymer nanocone array; and iv) controllable electrodeposition of the finishing active MnO_x layer (Figure 1A). An optical image of the as-prepared Au/MnO_x nanocone array electrode is shown in Fig 1B. It can be seen that a uniform Au/MnO_x nanocone array film as large as > 1 cm x 1 cm can be easily printed. In the actual device operation, a typical 1 cm x 1 cm refined area of the array was demarcated with a silicone rubber fixture. To construct an anodic alumina membrane (AAM) with an inverted nanocone hole array templates, four cycles of anodization and three cycles of etching were carried out as detailed in Supporting Information (SI, Figure S1). As shown in the scanning electron microscopy (SEM) cross-sectional and top view images (Figure 2A), the as-prepared mold is an inverted nanocone hole array with a length of ~1.7 μm and an open diameter of ~580 nm. The aspect ratio is close to 3, meaning a large enhancement in loading mass per unit area. We transferred the inverted nanocone hole array on AAM (the mold) into a perfluoropolyether (PFPE) substrate by UV-curing the photocurable pre-polymer. Owing to its low surface energy and good elasticity, the PFPE film patterned with the 3D nanocone array could be directly peeled off from the template without visible damage. Indeed, SEM image (Figure 2B) clearly reveals a perfectly inverted PFPE replica of the AAM template, demonstrating that PFPE is quite suitable for nanoscale molding from AAM patterns. Interestingly, with the 3D nanocone array pattern, the surface of PFPE was found to be superhydrophobic (SI, Figure S2). Remarkably, the template could be used several hundred times without any noticeable structural collapse due to the mechanical robustness of the template and the soft nature of the contact printing process. The inherently excellent chemical stability of PFPE facilitated the following fabrication processes. To obtain a highly conductive electrode for the current collector, we deposited Au metal by magnetron sputtering and the conformal coating of Au on the 3D nanocone array is clearly evidenced in the SEM image in Figure 2C. Note that the cone morphology is vital for achieving the conformal coating by sputtering and that is why we designed the template with an inverted nanocone hole array architecture in the first place. With the square array architecture, we have prepared templates with various lengths and diameters without any complicated processes or expensive equipments,[22-23] and hence desirable nanocone arrays of high aspect ratios (i.e., large surface areas) for pseudocapacitor electrodes could be readily obtained by tuning the imprint pitches and anodization conditions.

The next step completes the 3D nanocone array electrode by controllably electrodepositing MnO_x nanosheets. Figure 2D-G show that the electrodeposited MnO_x nanosheets have been homogeneously coated on each nanocone and different thicknesses could be obtained by varying the deposition time; to be more precise, the longer the deposition time, the thicker the MnO_x film (see the high-magnification SEM images in Figure S3). TEM images in Figure S4 clearly show that each nanocone is comprised of numerous ultrathin nanosheets. Glancing angle X-ray diffraction (XRD) pattern and Raman scattering spectra (SI, Figure S5) revealed the complicated phase of the ultrathin nanosheets of MnO_x. The broad Raman band around 648 – 575 cm^{-1} results from the overlap of MnO_x characteristic peaks;[24] they can be assigned to the Mn-O breathing vibration of divalent Mn ions in tetrahedral coordination and the Mn-O stretching vibration of the MnO_6 octahedra. Furthermore, in the high-resolution X-ray photoelectron spectra (XPS), two major peaks with binding energies at 642.0 eV and 653.8 eV correspond to Mn $2p_{3/2}$ and Mn $2p_{1/2}$, respectively. The O 1s XPS spectral features located in the range of 527.5 - 533.5 eV can be plausibly attributed to Mn oxide (Mn-O-Mn), Mn hydroxyl (Mn-OH) and residue water (H-O-H). Therefore, the MnO_x phase we prepared could contain Mn_3O_4, MnOOH, etc.[24-26] It has been reported that alkaline or proton ions could migrate in manganese oxide by hopping between the H_2O and OH^- sites.[3] This suggests that increasing the H_2O/OH^- hopping sites is crucial for improving the ion conductivity.[26]

To evaluate the electrochemical behaviours of the 3D Au/MnO_x nanocone array electrodes, we performed cyclic voltammetry (CV) measurements with a three-electrode configuration in a 1 M Na_2SO_4 electrolyte in a voltage window between 0 and 0.8 V. Figure 3A presents typical CV curves of the Au/MnO_x electrodes with different deposition time at a scan rate of 50 mV s^{-1}. Note that the Au electrode without the active MnO_x material shows almost negligible capacitance. However, the other electrodes with the active MnO_x material respond with appreciable capacitance and significantly, the corresponding CV curves appear nearly

View Article Online
DOI: 10.1039/C3NR06675D

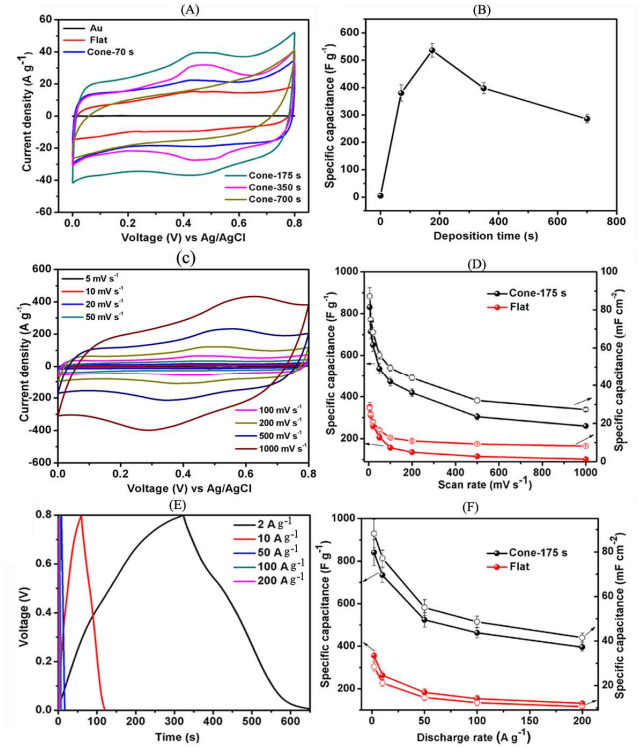

Figure 3. **Electrochemical characterizations of the Au/MnO_x nanocone array electrode.** A, Comparisons of CV curves of Au/MnO_x electrode obtained in different deposition time at a scan rate of 50 mV s^{-1} in 1M Na_2SO_4, showing the best performance achieved in the deposition time of 175 s. B, Calculated specific capacitances of Au/MnO_x nanocone array electrode in different deposition time at a scan rate of 50 mV s^{-1} in 1M Na_2SO_4. C, CV curves of Au/MnO_x nanocone array electrode in the deposition time of 175 s at various scan rates. D, Specific capacitances of Au/MnO_x nanocone array electrodes and flat electrodes as a function of different scan rates. E, Charge-discharge curves of Au/MnO_x nanocone array electrode in the deposition time of 175 s at various current densities. F, Specific capacitance of Au/MnO_x nanocone array electrodes and flat electrodes as a function of different current densities. They showed that both mass capacitances and area capacitances of Au/MnO_x nanocone array electrodes are much larger than that of flat electrode.

rectangular, implying a nearly ideal capacitive behavior. In addition, a pair of symmetric (nearly reversible at low scan rates) anodic and cathodic peaks is observed for the films with the MnO_x deposition time ranging from 70 to 700 s, suggesting that the faradic surface charge storage in thinner MnO_x nanosheets is excellent. From the areas of the CV curves (A), specific capacitance C (F g^{-1}) was calculated by $C = A/2mv\Delta V$ (F g^{-1}), where m is mass of electroactive material (g), v potential scan rate (V s^{-1}), and ΔV = cathodic potential (V_c) – anodic potential (V_a). The highest specific capacitance of 536.1 F g^{-1} was obtained with the 3D array of 175 s deposition time (MnO_x mass: ~0.110 mg cm^{-2}) at a scan rate of 50 mV s^{-1}. With a longer deposition time of 700 s, however, the specific capacitance dropped to 285.5 F g^{-1} (Figure 3B) clearly resulting from the poor intrinsic conductivity of MnO_x and the electrolyte diffusion limitation in a more restricted space.

Based on the above observations, the Au/MnO_x nanocone array electrode deposited with 175 s was further investigated at various CV scan rates from 5 to 1000 mV s^{-1} (Figure 3C). Again, the rectangular CV curves are indicative of the excellent capacitive characteristics of the electrode. The specific capacitance is calculated to be 830.6, 714.1, 650.2, 536.2, 471.3, 418.6, 304.5 and 253.5 F g^{-1}, respectively, in the order of increasing scan rate of 5, 10, 20, 50, 100, 200, 500 and 1000 mV s^{-1}. In contrast, the flat electrode with the same mass loading only shows a specific capacitance of 350.4 F g^{-1} at a low scan rate of 5 mV s^{-1} and 103.1 F g^{-1} at a high scan rate of 1000 mV s^{-1}. Thus the capacitive values of the Au/MnO_x nanocone array electrode are enhanced by about 2.4 times over those of the flat electrode at identical scan rates (Figure 3D). In terms of areal specific capacitance, the corresponding enhancement factor is about 3.2. For example, the calculated value is 87.2 mF cm^{-2} for the nanocone array electrode and 28.0 mF cm^{-2} for the flat electrode at a scan rate of 5 mV s^{-1}. This enhancement clearly shows the advantage of the high aspect ratio nanocone arrays.

To more directly probe the capacitive response of the Au/MnO_x nanocone array electrodes, galvanostatic charging/discharging measurements were performed in 1 M Na_2SO_4 solution using a Pt counter electrode and an Ag/AgCl reference electrode. The specific capacitance was calculated from the discharge curve based on the equation $C = -I(\Delta V/\Delta t)^{-1}$ (F g^{-1}), where I is the current density (A g^{-1}) and $\Delta V/\Delta t$ is the slope of the discharge curve. Figure 3E presents the charge-discharge curves at various current densities from 2 to 200 A g^{-1} in the voltage window between 0 and 0.8 V. These curves are consistent with the CV curves described above in terms of the reversibility and the redox features. The specific capacitances of the Au/MnO_x nanocone array electrode and the flat electrode at a current density of 2 A g^{-1} are 840.3 F g^{-1} (88.2 mF cm^{-2}) and 355.2 F g^{-1} (28.4 mF cm^{-2}), respectively. When the current density rises up to 200 A g^{-1}, the specific capacitance of the Au/MnO_x nanocone array electrode still retains 395.6 F g^{-1}, whereas it is only 131.2 F g^{-1} for the flat electrode at the same current density, suggesting remarkable rate performance of our unique 3D Au/MnO_x nanocone array electrode. Noticeably, the best specific capacitance with high mass loading is higher than those reported previously using core-shell nanowires and nanotubes of MnO_x.[18-21,27]

Considering the remarkable specific capacitance and rate capability of our purpose-built Au/MnO_x nanocone array electrode and electrostatic storage of the electrical energy for graphene sheet material, an asymmetric supercapacitor based on these structures have been assembled to obtain a more realistic evaluation of the capacitive performance. Reduced graphene oxide (RGO), also called chemically converted graphene (CCG), was prepared according to our previous reports.[28-31] With a large capacitance at the ultrahigh current density, CCG hydrogel films could be supplied with an ideal counter electrode.[31]

Prior to evaluating an asymmetric capacitor, CV measurements of the individual Au/MnO_x nanocone array electrode and CCG electrode in 1 M Na_2SO_4 solution were performed using a Pt counter electrode and a Ag/AgCl reference electrode at a scan rate of 5 mV s^{-1}. Calculated from CV curves, the specific capacitance of the Au/MnO_x nanocone array electrode is 854.6 F g^{-1} within a potential window of 0 to 0.8 V (vs. Ag/AgCl) and that of CCG electrode is 214.5 F g^{-1} within a potential window of -1 to 0 V (vs. Ag/AgCl) (SI, Figure S6). This suggests that the full cell voltage can be extended up to 1.8 V in 1 M Na_2SO_4 solution for the asymmetric supercapacitor.[32] It should be emphasized here that the operation at higher voltages can clearly deliver higher energy and power densities. A higher operation voltage corresponds to a higher overall performance of the supercapacitor, as the energy and power are proportional to the square of the voltage ($E = 1/2CV^2$ and $P = E/t$, where C is the full cell capacitance, V is the voltage and t is the discharge time). Additionally, operation at higher voltages means that in practical

View Article Online
DOI: 10.1039/C3NR06675D

applications, one can reduce the number of supercapacitors in series required to reach the desired output voltage.

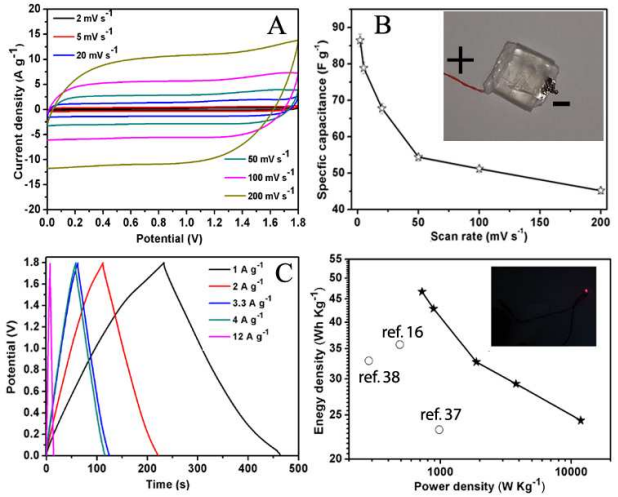

Figure 4. **Performance testing of a full supercapacitor consisting the 3D Au/MnO_x nanocone array positive electrode and the CCG negative electrode.** A, CV curves of the full supercapacitor at various scan rates in 1 M Na_2SO_4. B, Corresponding specific capacitance as a function of scan rates. C, Charge-discharge curves at various current densities. D, Energy density as a function of power density. Inset of B: a full supercapacitor assembly; Inset of D: the asymmetric supercapacitor can lighten up a red LED indicator (1.8 V).

The assembly of a well-performed electrochemical supercapacitor should take into account the charge balance between the two electrodes,[33] and the relationship of the charges between the two electrodes is $Q_+ = Q_-$, $Q = C_s * m * \Delta V$, where C_s is the specific capacitance, m is the mass of the active material, and ΔV is the potential range. Thus, on the basis of the specific capacitance values and potential windows found for the Au/MnO_x nanocone array electrode and RGO/graphite electrode, the optimal mass ratio between the two electrodes should be $m_{(Au/MnOx)}/m_{(RGO)}$ = 0.313 in the asymmetric supercapacitors. In the assembled asymmetric supercapacitors for testing, Au/MnO_x nanocone array was used as a positive electrode and CCG hydrogel film/Pt as a negative electrode in a 1 M Na_2SO_4 solution, separated by a wet glass fibre, as shown in the inset of Figure 4B.

Figure 4A presents CV curves of an optimized asymmetric supercapacitor at different scan rates from 2 to 200 mV s^{-1}. These CV curves still remain rectangular shape with increasing scan rates, even at a high scan rate of 200 mV s^{-1}, confirming again a nearly ideal capacitive behaviour. The calculated cell capacitance gradually decreases from 86.5 to 45.2 F g^{-1} with increasing scan rates (Figure 4B). At high scan rates, the diffusion of the electrolytic ions into the deep valleys is hindered, and thus only the outer surface of the active material is used for charge storage. Galvanostatic cycling of the asymmetric supercapacitor electrodes was performed at various current densities in the voltage range of 0-1.8 V (Figure 4C). The specific capacitances obtained were 108.5, 101.9, 81.5, 75.6 and 68.4 F g^{-1} at current densities of 1.0, 2.0, 3.3, 4.0 and 12.0 A g^{-1}, respectively. The value gradually decreases with increasing current densities, in a way similar to the CV results.

Good capacitance retention is crucial to the practical application of supercapacitors.[34-36] The cycling performance of the optimized asymmetric supercapacitor over 2000 charge/discharge was performed at a current density of 2 A g^{-1} (SI, Figure S7). A total capacitance decay of only 3.5% is observed, indicating the excellent long-term stability of the asymmetric capacitor. The relationship between energy density and power density is also shown (Figure 4D). Particularly remarkable are the energy density values from 46.8 to 24.3 Wh Kg^{-1} and the corresponding power densities increasing from 0.72 to 11.83 kW Kg^{-1}. It is worth pointing out that this result in terms of energy density and power density surpasses those of most other asymmetric supercapacitors reported to date. [16,37,38] Noticing that the capacitance of asymmetric supercapacitors is largely limited by the carbon-based negative electrode, further capacitance enhancement is possible by, for example, improving the capacitance of the carbon-based negative electrode or using new high capacitance material as the negative electrode.

In summary, we have achieved a remarkable capacitive performance of an asymmetric supercapacitor using a purpose-built 3D Au/MnO_x nanocone array as the positive electrode and the CCG electrode as the negative electrode. The 3D Au/MnO_x nanocone array electrode was obtained a specific mass (areal) capacitance of 840.3 F g^{-1} (88.2 mF cm^{-2}) at a current density of 2 A g^{-1}, which is much higher than that of the flat electrode, only 355.2 F g^{-1} (28.4 mF g^{-1}). Additionally, when assembled into an asymmetric supercapacitor, a cell capacitance of 108.5 F g^{-1} was achieved at a current density of 1 A g^{-1}, and the corresponding energy density is as high as 46.8 Wh Kg^{-1} at a power density of 0.72 kW Kg^{-1}. After 2000 cycles of charge-discharge, the cell capacitance still remained 96.5% of the initial capacitance. Additionally, we have also electrodeposited other electrochemically active materials such as $Ni(OH)_2$ and FeOOH on the purpose-built 3D Au/MnO_x nanocone array electrode, which exhibited remarkable electrochemical performance as well. The excellent pseudocapacitive performance highlights the importance of the 3D electrode design with the enhanced charge transport kinetics but without compromising the loading of the active materials involved, thereby boosting both power density and energy density.

Several factors need be considered in the design of the high performance asymmetric supercapacitor. First, considering that the electrochemical capacitors largely depend on the surface structure and electronic conductivity of electrochemically active materials, our propose-built conductive nanocone array can address these issues by adjusting the pitches of nanocone arrays and controlling electrodeposition of oxides. For example, owing to the poor conductivity of MnO_x, approximately 120 nm thick MnO_x deposited on Au nanocone array electrode can achieve good capacitive performance at a relatively high scan rate of 50 mV s^{-1}. Second, our purpose-built 3D conductive electrode may largely shorten electron transportation distance and controllable electrodeposition of MnO_x can make electrolytic ions easily access to the active material. Third, the electrode with a larger contact area than the flat one results in the increase of electrochemically active sites for redox reaction. Fourth, although the capacitive performance of asymmetric supercapacitors is largely restricted by the carbon-based negative materials, the graphene-based material with a large surface area and electronic conductivity has been demonstrated to improve the cell capacitance of the asymmetric supercapacitor. Therefore, the significant advance demonstrated here for the first time indicates that the purpose-built 3D Au/MnO_x nanocone array is a promising electrode substrate for building up efficient electrochemical pseudocapacitors. This will open new avenues for developing high-performance supercapacitors and other energy-storage devices.

View Article Online
DOI: 10.1039/C3NR06675D

This work was supported by the HK-RGC General Research Funds (GRF No. HKUST 605710, 604809 and 612111), partially supported by ITS/192/11 from Hong Kong Innovation Technology Commission, HKUST Research Project Competition Grant (RPC11EG38), and NSFC No. 21303251.

Notes and references

[†]*Nano Science and Technology Program, Department of Chemistry, The Hong Kong University of Science and Technology, Clear Water Bay, Kowloon, Hong Kong (P. R. China),* [‡] *Department of Electronic and Computer Engineering, The Hong Kong University of Science and Technology, Clear Water Bay, Kowloon, Hong Kong (P. R. China),* [§]*i-LAB, Suzhou Institute of Nano-Tech and Nano- Bionics, Chinese Academy of Science, China *CORRESPONDING AUTHOR E-mail: (ygzhang2012@sinano.ac.cn) (eezfan@ust.hk) (chsyang@ust.hk)*

Electronic Supplementary Information (ESI) available: (1) Experimental section; (2) additional SEM, TEM, XPS, and electrochemical testing data are included. See DOI: 10.1039/b000000x/

1. G. P. Wang, L. Zhang, J. J. Zhang, *Chem. Soc. Rev*. 2012, **41**, 797.
2. J. R. Miller, P. Simon, *Science* 2008, **321**, 651.
3. M. Winter, R. J. Brodd, *Chem. Rev.* 2004, **104**, 4245.
4. P. Simon, Y. Gogotsi, *Nat. Mater.* 2008, **7**, 845.
5. J. M. Tarascon, M. Armand, *Nature* 2001, **414**, 359.
6. Z. N. Yu, B. Duong, D. Abbitt, J. Thomas, *Adv. Mater.* 2013, **25**, 3302.
7. X. Y. Lang, A. Hirata, T. Fujita, M. W. Chen, *Nat. Nanotechnol.* 2011, **6**, 232
8. Q. Lu, M. W. Lattanzi, Y. P. Chen, X. M. Kou, W. F. Li, X. Fan, K. M. Unruh, J. G. G. Chen, J. Q. Xiao, *Angew. Chem. Int. Edit.* 2011, **50**, 6847.
9. K. K. Lee, S. Deng, H. M. Fan, S. Mhaisalkar, H. R. Tan, E. S. Tok, K. P. Loh, W. S. Chin, C. H. Sow, *Nanoscale* 2012, **4**, 2958.
10. C. Zhou, Y. W. Zhang, Y. Y. Li, J. P. Liu, *Nano Lett.* 2013, **13**, 2078.
11. S. P. Yu, X. C. Chang, Z. M. Wang, K. F. Han, H. Zhu, Advanced Materials, Pts 1-4 2011, 239-242, 2042.
12. S. K. Mondal, N. Munichandraiah, J Power Sources 2008, 175, 657.
13. H. L. Wang, H. S. Casalongue, Y. Y. Liang, H. J. Dai, *J. Am. Chem. Soc.* 2010, **132**, 7472.
14. L. Q. Mai, F. Yang, Y. L. Zhao, X. Xu, L. Xu, Y. Z. Luo, *Nat. Commun.* 2011, 2.
15. H. L. Wang, Y. Y. Liang, M. Gong, Y. G. Li, W. Chang, T. Mefford, J. G. Zhou, J. Wang, T. Regier, F. Wei, H. J. Dai, *Nat. Commun.* 2012, 3.
16. H. B. Li, M. H. Yu, F. X. Wang, P. Liu, Y. Liang, J. Xiao, C. X. Wang, Y. X. Tong, G. W. Yang, *Nat. Commun.* 2013, 4.
17. J. W. Xiao, S. Yang, L. Wan, F. Xiao and S. Wang, *J. Power Sources*, 2013, **245**, 1027.
18. Y. M. He, W. J. Chen, X. D. Li, Z. X. Zhang, J. C. Fu, C. H. Zhao, E. Q. Xie, *Acs Nano* 2013, **7**, 174.
19. G. H. Yu, L. B. Hu, N. A. Liu, H. L. Wang, M. Vosgueritchian, Y. Yang, Y. Cui, Z. A. Bao, *Nano Lett.* 2011, **11**, 4438.
20. X. H. Lu, T. Zhai, X. H. Zhang, Y. Q. Shen, L. Y. Yuan, B. Hu, L. Gong, J. Chen, Y. H. Gao, J. Zhou, Y. X. Tong, Z. L. Wang, *Adv. Mater.* 2012, **24**, 938.
21. J. A. Yan, E. Khoo, A. Sumboja, P. S. Lee, *Acs Nano* 2010, **4**, 4247.
22. Q. F. Lin, S. F. Leung, K. H. Tsui, B. Hua, Z. Y. Fan, *Nanoscale Res. Lett.* 2013, 8.
23. Q. F. Lin, B. Hua, S. F. Leung, X. C. Duan, Z. Y. Fan, *Acs Nano* 2013, **7**, 2725.
24. K. W. Nam, K. B. Kim, J Electrochem Soc 2006, 153, A81.
25. F. Buciuman, F. Patcas, R. Craciun, D. R. T. Zahn, *Phys. Chem. Chem. Phys.* 1999, **1**, 185.
26. F. Xiao, Y. L. Xu, *Int. J. Electrochem. Soc.* 2012, **7**, 7440.
27. J. P. Liu, J. Jiang, C. W. Cheng, H. X. Li, J. X. Zhang, H. Gong, H. J. Fan, *Adv. Mater.* 2011, **23**, 2076.
28. Y. C. Qiu, X. F. Zhang, S. H. Yang, *Phys. Chem. Chem. Phys.* 2011, **13**, 12554.
29. Y. C. Qiu, K. Y. Yan, S. H. Yang, L. M. Jin, H. Deng, W. S. Li, *Acs Nano* 2010, **4**, 6515.
30. J. W. Xiao, S. H. Yang, *J. Mater. Chem.* 2012, **22**, 12253.
31. X. W. Yang, C. Cheng, Y. F. Wang, L. Qiu, D. Li, *Science* 2013, **341**, 534.
32. Z. J. Fan, J. Yan, T. Wei, L. J. Zhi, G. Q. Ning, T. Y. Li, F. Wei, *Adv. Funct. Mater.* 2011, **21**, 2366.
33. V. Khomenko, E. Raymundo-Pinero, F. Beguin, *J. Power Sources* 2006, **153**, 183.
34. Y. Hou, Y. W. Cheng, T. Hobson, J. Liu, *Nano Lett.* 2010, **10**, 2727.
35. L. Q. Mai, H. Li, Y. L. Zhao, L. Xu, X. Xu, Y. Luo, Z. F. Zhang, W. Ke, C. J. Niu, Q. J. Zhang, *Sci. Rep.* 2013, **3**, 1718
36. H. Xia, D. Zhu, Z. Luo, Y. Yu, X. Q. Shi, G. L. Yuan, J. P. Xie, *Sci. Rep.* 2013, **3**, 2978.
37. H. Gao, F. Xiao, C. Ching, H. W. Duan, *ACS Appl. Mater. Interfaces,* 2012, **4**, 2801.
38. L. Chen, Z. Huang, H. Liang, Q. Guan, S. Yu, *Adv. Mater.* 2013, **25**, 4746.

View Article Online
DOI: 10.1039/C3NR06675D

Three-dimensional metal/oxide nanocone arrays for high-performance electrochemical pseudocapacitors

Yongcai Qiu, [†, ‡,§] Yihua Zhao, [†] Xiaowei Yang, [§] Wanfei Li, [§] Zhanhua Wei, [†] Qingfeng Lin, [‡] Hongkai Wu, [†] Yuegang Zhang, [§,*] Zhiyong Fan, [‡,*] Shihe Yang [†,*]

Three-dimensional (3D) electrodes are critical to enabling high-performance power sources. We report here on the design and fabrication, by combining imprint and soft-printing technologies, of 3D nanocone arrays as a novel platform for high performance pseudocapacitors.